



ELSEVIER

1 December 1998

OPTICS
COMMUNICATIONS

Optics Communications 157 (1998) 155–160

Ring cavity enhanced second harmonic generation of a diode laser using LBO crystal

T. Kaing^{*}, M. Houssin

Laboratoire de l'Horloge Atomique, Unité propre de Recherche du CNRS associée à l'Université de Paris-Sud, Université de Paris-Sud, Bât. 221, F-91405 Orsay Cedex, France

Received 6 May 1998; revised 20 July 1998; accepted 4 August 1998

Abstract

We report on a lithium triborate (LBO) second harmonic generator delivering up to 6- μ W usable power at 397 nm out of 33 mW of a 794-nm diode laser radiation. The LBO crystal is placed in an external ring cavity, compensated for astigmatism and coma, to enhance the fundamental power. Three cavity input couplers were tested for impedance-matching. With the best cavity, the enhancement factor of 1.5 is measured for 794-nm radiation, leading to an enhancement factor of 225 for the 397-nm beam. © 1998 Elsevier Science B.V. All rights reserved.

PACS: 42.55.P; 42.62; 42.65.K

Keywords: Enhancement cavity; Second harmonic generation; Aberration; Optical frequency standard; Diode laser

1. Introduction

In high-resolution spectroscopy of alkaline atoms and ions whose electronic resonance transitions are in the UV region, we need continuous, tunable, narrow line-width sources in this domain. Diode lasers are continuous-wave, tunable and compact sources. Unfortunately, nowadays, they can only access visible and infrared radiations. Second harmonic generation (SHG) in nonlinear crystals is then an alternative to extend the spectral range accessible with diode lasers to the UV region. Recently, several authors have reported external-cavity enhanced SHG in this region using diode laser as fundamental source [1–4].

For the realization of an optical frequency standard, Ca^+ ion is a promising candidate [5]. It has a red transition with a very narrow natural line-width, which can be actually observed with very small perturbation in a Paul trap. Moreover, all the useful transitions involved in the experiment can be reached with laser diodes, yielding a reliable

and compact setup. Laser cooling and observation of these ions require a source at 397 nm. Since this wavelength is not available with commercial laser diodes, it can be generated by SHG of a 794-nm laser diode radiation using nonlinear bulk crystals. To double an 842-nm radiation, Hammerich et al. [1] used KNbO_3 because it has a large nonlinear susceptibility [6,7]. However, the 90° noncritical phase-matching wavelength in this crystal can only be temperature tuned until 838 nm for $T = -36^\circ$ [8]. Below this temperature, KNbO_3 undergoes a phase transition. Hence, SHG of a 794-nm radiation is not possible in this crystal. Apart from KNbO_3 , the other classical crystals do not present the optimal 90° noncritical phase-matching condition at 794 nm. With critical phase-matching, the mostly used crystals for SHG in the UV region are LiIO_3 , BBO and LBO. These crystals, compared to other UV crystals (KDP, ADP), have larger optical nonlinearity. Performances of these crystals are summarised in Table 1 where the theoretical conversion efficiency γ_{SH} is calculated using Ref. [9] for 1.4-cm crystal length.

The LiIO_3 crystal has a large nonlinear coefficient, but its large walk-off angle, small acceptance angle and hysteresis make it difficult to use. As LiIO_3 , BBO crystal

^{*} Corresponding author. Laboratoire Primaire du Temps and des Fréquences, Observatoire de Paris, 61 Avenue de l'Observatoire, 75014 Paris, France. E-mail: to.kaing@obspm.fr

Table 1
Comparison of three UV crystal performances for SHG

Crystal	LiIO ₃	BBO	LBO
Transparency window	0.3–6 μm	0.19–2.6 μm	0.16–2.6 μm
n_o	1.87	1.69	1.61
Phase-matching angle (deg) for type I oo → e	42	27	$\varphi = 32, \theta = 90$
Walk-off (deg)	5	3.9	1
d_{eff} (Definition)	$d_{31}\sin\theta$	$d_{22}\cos\theta$	$d_{32}\cos\varphi$
d_{ij} (pm/V) [6,7]	$d_{31} = -4.10$	$d_{22} = 2.22$	$d_{32} = 1.17$
d_{eff} (pm/V)	2.7	1.9	1.0
γ_{SH} ($\times 10^{-4} \text{ W}^{-1}$) [9]	1.40	1.18	1.26

has large walk-off angle, which limits the aperture length of the crystal. Though LBO has a smaller nonlinear susceptibility, it is more convenient to use due to its very small walk-off angle, large angle and wavelength acceptances, and high damage threshold. And although this crystal has been shown to be the most suitable material for frequency doubling in the 700–850-nm region [10], it is not frequently used, especially to double diode laser radiation.

To have a compact, portable and tunable source, diode lasers are needed for SHG. But, due to low power of these diodes (typically up to 100 mW), and to the small conversion efficiency γ_{SH} (cf. Table 1), the μW-level of the UV power required to detect and cool the Ca⁺ ions [11,12] cannot be obtained by single pass doubling. The use of an external passive resonator is hence needed to enhance the generated harmonic power.

This paper reports on our experimental results obtained with a resonant external ring cavity used to frequency double the 794-nm radiation from a 100-mW AlGaAs diode laser. The astigmatism and coma-compensated shape of the cavity, the impedance and mode-matching, and the stabilization of a cavity resonance frequency to the laser frequency will be discussed.

2. Theoretical determination of the cavity parameters

2.1. Astigmatism and coma compensation

To limit cavity losses by inserting the nonlinear crystal, the latter is cut at Brewster angles for the 794-nm radiation. In focusing through a Brewster angled surface, astigmatism and coma are introduced. Astigmatism distortion limits the performance of SHG and coma degrades the focus in the crystal and introduces linear losses inside the cavity. Our ring enhancement cavity is designed to minimise these astigmatism and coma aberrations. Also, the distance between the two curved mirrors is chosen to assure cavity stability and to optimise the waist in the crystal for SHG. As shown by Kogelnik et al. [13], astigmatism can be compensated by the use of off-axis focusing

mirrors. Also, Dunn and Ferguson [14] present an unusual cavity design (Fig. 1) that enables both aberrations to be eliminated, both in the crystal and overall.

Astigmatism introduced by reflection at one Brewster angled surface can be compensated by one reflection at one of the off-axis mirrors for the angle of incidence $I = I_{\text{corr}}$. Good focus as well as overall cavity stability are preserved. If ρ is the radius of curvature of the spherical mirror, n is the refraction index of the crystal, t is the crystal length measured normally to the inclined facets of the crystal, the condition for astigmatism compensation is:

$$\rho \tan I_{\text{corr}} \sin I_{\text{corr}} = \frac{t(n^2 - 1)\sqrt{n^2 + 1}}{n^4}.$$

For $\rho = 10$ cm, $t = 1.4$ cm, $n = 1.6$, we find $I_{\text{corr}} = 14.3^\circ$.

Astigmatism compensation is independent of the sign of the crystal orientation. On the other hand, since the coma is an odd function of the angle I , the orientation of the crystal is important for coma compensation or reduction. Because the size of the different mountings limits the minimum value of ρ , coma cannot be also compensated but it is reduced with the asymmetric arrangement of mirrors M_2 and M_3 around the crystal. The residual coma Δx in the focal plane within the crystal is:

$$\Delta x = 6n \left(\rho \sin I - \frac{2t(n^4 - 1)\sqrt{n^2 + 1}}{n^7} \right) \delta^2,$$

where 4δ is the far field diffraction angle and can be written as: $4\delta = \lambda/\pi w_0$, w_0 is the cavity waist inside the crystal.

This residual coma induces a degradation of the cavity focus. This degradation is composed of a spatial asymmetric deformation and an extent. It is equivalent to an inaccurate mode-matching. To evaluate it, we compare the residual coma Δx to the beam waist determined by the cavity. For a cavity with a shape described in Fig. 1 and with length L , the average waist w_0 within the crystal in the stability range of the cavity verifies [14]:

$$w_0^2 = \frac{\lambda}{2\pi} \frac{\rho^2}{2(L - \rho)}.$$

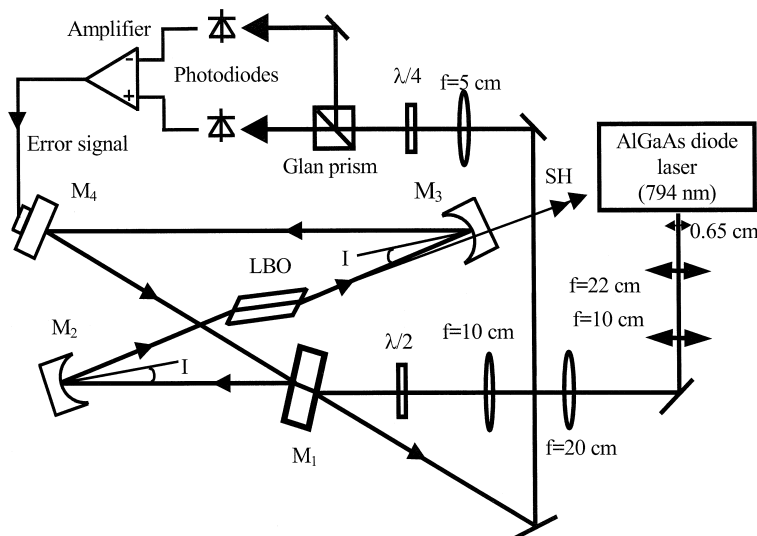


Fig. 1. Experimental setup showing the ring enhancement cavity and the stabilisation of the cavity length to the laser frequency.

Then, for $L = 50$ cm, $\rho = 10$ cm, $n = 1.6$, $\lambda = 794$ nm, we find $w_0 = 40 \mu\text{m}$ and $\Delta x/w_0 = 0.8\%$ per round-trip in our cavity. For a more classical ring enhancement cavity with the same parameters and with no coma compensation, it would have been $\Delta x/w_0 = 2.2\%$. For the Gaussian mode TEM_{00} of the cavity, if the waist deformation due to coma after a round trip in the cavity is modelised by a Δx extent combined with a Δx shift, we calculate $2 \times (\Delta x/w_0)^2$ extra losses per round trip. This result means 0.01% extra losses for our cavity and 0.1% extra losses for a classical cavity. As we show further in Section 4, such extra losses can be significant.

2.2. Impedance-matching

The enhancement of power in a ring resonant cavity depends on the transmission of the coupling mirror and the total losses inside the cavity. These losses are due to the less than 100% reflectivity of the three highly reflecting mirrors, to the absorption and scattering in the crystal, and to the conversion of the fundamental power into harmonic power. If R is the input mirror reflectivity (and T its transmission factor) and l describes the intra-cavity losses, the enhancement factor κ can be expressed by [15,16]:

$$\kappa = \frac{1 - R}{(1 - \sqrt{R(1 - l)})^2} \approx \frac{4T}{(T + l)^2} \text{ for } T, l \ll 1.$$

One can see that the enhancement factor reaches its maximum value when R is equal to $(1 - l)$ or when the transmission T is equal to l (impedance-matching). Because of poor spatial qualities of diode laser light, mode-matching is quite more delicate than with dye or

titanium-sapphire lasers which have very good TEM_{00} mode. If we call η the mode-matching factor, the real enhancement factor is $S = \eta\kappa$.

3. Experiment

The experimental setup is presented in Fig. 1. After a collimating lens, and an afocal system of cylindrical lenses to circularize the beam profile, the 794-nm radiation is mode-matched to the cavity with two spherical lenses of 20 and 10 cm focal lengths. The spacing between these lenses can be adjusted by translation stages to optimise the mode-matching.

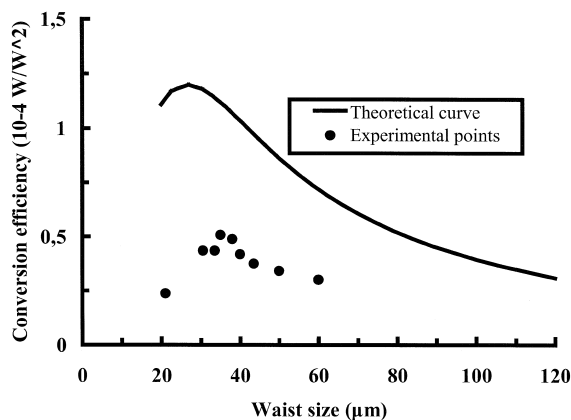


Fig. 2. Theoretical and experimental dependence of the harmonic power on the fundamental beam waist size within the crystal.

The bow-tie ring enhancement cavity is made of two planar mirrors (M_1 and M_4) and two curved mirrors (M_2 and M_3) with 10-cm radius of curvature. The mirror M_1 is an input coupler with a transmission factor T at 794 nm. The coupling efficiency depends on this factor T which allows to impedance-match the total losses inside the cavity. One of the two curved mirrors (M_3) is a dichroic mirror. It transmits 90% of the 397-nm radiation and reflects 99.9% of the 794-nm radiation. The other two mirrors M_2 and M_4 have their reflectivity nearly equal to 1 at the fundamental 794-nm radiation. The optical length of the cavity is 50 cm. The whole cavity is placed upon a plate to isolate from vibrations.

The 1.4-cm-long LBO crystal is cut at Brewster angle for horizontal polarization and at 32.28° internal angle for type I ($oo \rightarrow e$) phase-matching. The losses at Brewster angle for the 794-nm beam are measured to be 0.7% at the optimum phase-matching angle. The crystal is put between the two curved mirrors (M_2 and M_3) which are supported

by translation stages. The distance between M_2 and M_3 is chosen to assure the stability of the cavity and to optimise the size of the waist in the center of the crystal so that the conversion efficiency of the SHG is maximised. Fig. 2 shows the conversion efficiency versus the waist sizes. In this figure, the experimental points are obtained by single pass SHG and the corresponding waist sizes are the measured ones. The experimental and theoretical optimum waist sizes at the center of the crystal are about 33 and 27 μm , respectively. The difference between the two optima is due to the fact that a Gaussian beam is supposed for theoretical calculations while in reality diode laser beams are astigmatic.

The planar mirror M_4 is supported by a piezoelectric transducer (PZT) which permits to scan the cavity length over 4 GHz and to adjust this length so that a peak of the cavity resonance optically locks to the laser frequency. The locking scheme is a technique using a polarization spectroscopy of the reflected beam from the cavity [17]. A $\lambda/2$ plate is placed in front of the cavity to give a small angle to the polarization of the incident radiation with respect to the polarization of the ring cavity defined by the Brewster facets of the LBO crystal. The reflected light acquires a frequency-dependent elliptical polarization. A polarization analyzer formed by a $\lambda/4$ retarder and a Glan prism detects the dispersion shaped resonances which give the signal error for electronic frequency stabilization. Fig. 3a shows an example of an error signal registered by a numerical oscilloscope.

4. Results

As previously noted, the enhancement factor of the 794-nm radiation in the cavity depends on the transmission factor T of mirror M_1 and on the intra-cavity losses. We use three input couplers with measured T_C equal to 1.5, 4.6 and 5.9% to test the impedance-matching to intra-cavity losses. For each coupler, we measure the resonant reflectivity of the cavity $R_R = P_s/P_{ns}$ (where P_s is the mirror M_1 reflected power when the cavity is resonant for the fundamental light and P_{ns} when the cavity is not resonant), the cavity finesse F_m , the real enhancement factor $S = P_{inside}/P_{in}$ (where P_{inside} and P_{in} are the 794-nm

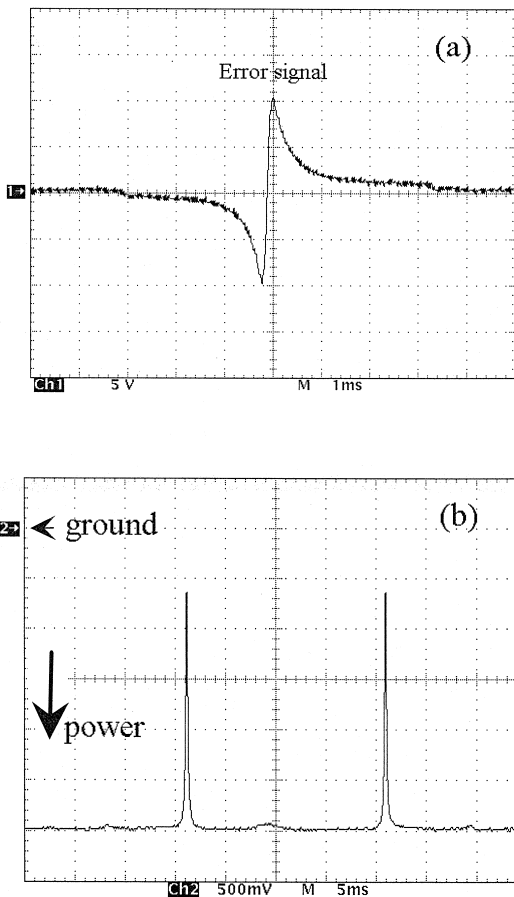


Fig. 3. (a) Example of an error signal for frequency stabilisation. (b) Optical power reflected at the coupling mirror input of the enhancement cavity showing the decreased resonance peak and the 80% mode-matching rate.

Table 2
Enhancement cavity properties

T_C (%)	R_R (%)	F_m	S	T_{eff} (%)	l (%)	κ	R_C (%)	η (%)
1.5	53	92	8.7	6.8	5.3	13	31	78.4
4.6	20	62	15	10.1	5.5	18	0.8	80.8
5.9	25	55	11.6	11.4	5.5	18	0.1	75.1

Left: experimental measurements; Right: extrapolated from experimental results.

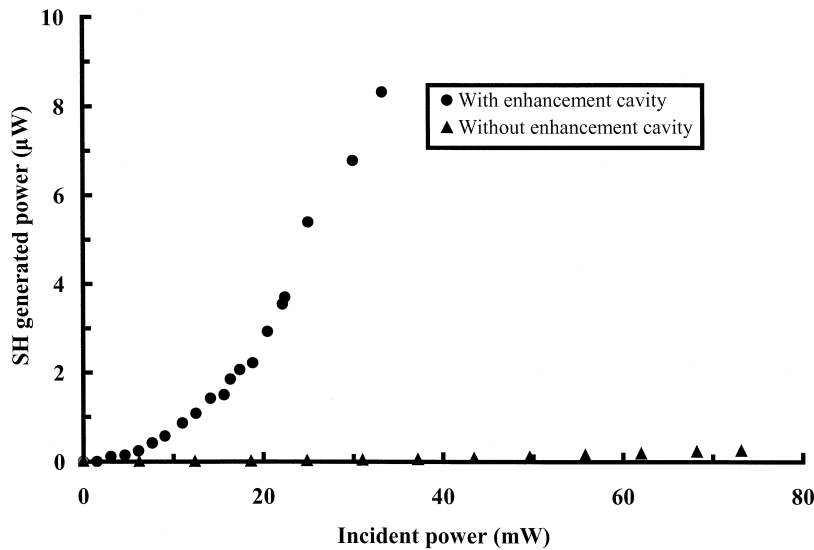


Fig. 4. Experimental SH power without and with the best enhancement cavity.

powers inside the cavity and at the cavity input). From these measurements, we retrieve [2,18] the relative power loss per round-trip T_{eff} ($T_{\text{eff}} = 2\pi/F_m$), the intra-cavity losses l ($l = T_{\text{eff}} - T_C$), the enhancement factor in the case of perfect mode-matching κ ($\kappa = 4T_C/T_{\text{eff}}^2$), the residual reflectivity due to impedance-mismatch R_C ($R_C = (T_{\text{eff}} - 2T_C)^2/T_{\text{eff}}^2$), and the mode-matching rate $\eta = 1 - (R_R - R_C)$. All these results are summarised in Table 2. The intra-cavity loss l is about 5.5%. This high factor is probably due to bad quality of the highly-reflection coating of our mirrors. The mode-matching rate is about 80%. The input coupler with $T = 1.5\%$ does not allow a good impedance-matching to cavity losses ($R_C = 31\%$), while the other two input couplers ($T = 4.6\%$ and $T = 5.9\%$) allow a perfect impedance-matching ($R_C < 1\%$). In the experimental situation, the highest observed mode-matching rate (Fig. 3b) is 80% ($R_R = 20\%$) for the coupler with $T = 4.6\%$. The latter is then the best coupler, and the total enhancement factor of the fundamental beam is then $S = \eta\kappa = 15$.

In our configuration, an addition of $l_c = 0.1\%$ losses due to coma leads to a $2l_c/T_{\text{eff}} = 2\%$ decrease of the enhancement factor. In our case, although the coma effect is small, the other intra-cavity losses are quite high (5.5%). Moreover, waist degradation due to coma increases when the cavity waist decreases. With a $33\text{-}\mu\text{m}$ waist, that optimises SHG, the residual relative coma $\Delta x/w_0$ becomes 1.4% in our configuration and 3.6% if coma is not compensated. The latter case leads to 0.22% extra losses per round trip due to coma. With the coma correction, the gain in the enhancement factor is 4.5% and in the blue power is 9%.

Fig. 4 shows the comparison of the generated harmonic powers (compensated for different losses) measured with-

out and with the best enhancement cavity. From these curves, the doubling efficiency coefficients are 0.44×10^{-4} and $7.80 \times 10^{-3} \text{ W/W}^2$, respectively. With the enhancement cavity, the corresponding theoretical efficiency is $\gamma = 20 \times 10^{-3} \text{ W/W}^2$. This efficiency γ is obtained by using γ_{SH} issued from Table 1 and by taking into account the enhancement factor of the cavity ($S = 15$), 20% loss due to the fact that the output facet of the crystal is not at Brewster angle for the 397-nm beam [19] and 10% loss due to the mirror M_3 . The difference between the experimental and theoretical values is due to the bad spatial qualities and the observed astigmatism of diode laser radiation, and to the errors caused by the difficulty in measuring the low level of the harmonic power.

The blue-generated output is a Gaussian beam issued from the TEM_{00} cavity mode. It is slightly divergent and has a 1×4.5 elliptical cross-section because of the walk-off angle. This elliptical cross-section can be reduced to $\sim 1 \times 1.3$ with two cylindrical lenses in an afocal configuration. It is then focused to a $90\text{-}\mu\text{m}$ waist in the center of the ion trap with two spherical lenses. From the diffraction formula, we calculate a $78\text{-}\mu\text{m}$ waist. The blue beam is hence a nearly time-diffraction-limited beam. The UV available power for the detection and the cooling of the Ca^+ ions is $2.4 \text{ }\mu\text{W}$.

5. Conclusion

We have used an efficient bow-tie ring enhancement cavity, compensated for astigmatism and coma, to generate $6\text{-}\mu\text{W}$ usable power of 397-nm radiation out of 33 mW of a diode laser output by SHG using LBO crystal. This UV

power level is enough to detect the S–P transition of Ca^+ ions [11], but still not sufficient to cool these ions (a 50- μW level would be necessary to saturate the S–P transition). To optimise the UV power generated, low loss optical elements should be used to replace the ones which were used to reshape the laser beam, in such a way to increase the 794-nm power in front of the cavity. Furthermore, the single diode laser can be advantageously replaced with an injection-locked master oscillator-power amplifier diode setup, delivering a 100-mW power and a 500-kHz level line-width. A grating-tuned-ECDL as the master oscillator will allow a continuous frequency tuning of the UV radiation around 397 nm for high-resolution spectroscopy of UV atomic transitions.

Acknowledgements

This work was supported by the Bureau National de Métrologie (BNM), Paris, France. The authors would like to thank M. Desaintfuscien and J.-J. Zondy for reading the manuscript and for their advices.

References

- [1] A. Hammerich, D.H. McIntyre, C. Zimmermann, T.W. Hänsch, *Optics Lett.* 15 (1990) 372.
- [2] Chr. Tamm, *Appl. Phys. B* 56 (1993) 295.
- [3] K. Hayasaka, M. Watanabe, H. Imajo, R. Ohmukai, S. Urabe, *Appl. Optics* 33 (1994) 2290.
- [4] M. de Angelis, G.M. Tino, P. de Natale, C. Fort, G. Modugno, M. Prevedelli, C. Zimmermann, *Appl. Phys. B* 62 (1996) 333.
- [5] F. Plumelle, M. Desaintfuscien, M. Houssin, *IEEE Trans. Instr. Meas.* 42 (2) (1993) .
- [6] V.G. Dmitriev, G.G. Gurzadyan, D.N. Nikogosyan, *Handbook of Nonlinear Optical Crystals*, Chap. 3, and references therein.
- [7] R.C. Eckardt, H. Masuda, Y.X. Fan, R.L. Byer, *IEEE J. Quantum Electron.* QE-26 (1990) 922–933.
- [8] J.C. Baumert, P. Günter, H. Melchior, *Optics Comm.* 48 (1983) 215.
- [9] G.D. Boyd, D.A. Kleinman, *J. Appl. Phys.* 39 (1968) 3597.
- [10] C.S. Adams, A.I. Ferguson, *Optics Comm.* 90 (1992) 89.
- [11] S. Urabe, H. Imajo, K. Hayasaka, M. Watanabe, *J. Mod. Optics* 39 (2) (1992) 417.
- [12] M. Knoop, J. Rink, M. Vedel, F. Vedel, *Proceeding of the 5th Symposium on Frequency Standards and Metrology*, 1995, pp. 430–431.
- [13] H.W. Kogelnik, E.P. Ippen, A. Dienes, C.V. Shank, *IEEE J. Quantum Electron.* QE-8 (1972) 373.
- [14] M.H. Dunn, A.I. Ferguson, *Optics Comm.* 20 (1977) 214.
- [15] M. Brieger, H. Busener, A. Hese, F.v. Moers, A. Renn, *Optics Comm.* 38 (1981) 423.
- [16] J.C. Bergquist, H. Hemmati, W.M. Itano, *Optics Comm.* 43 (1982) 437.
- [17] T.W. Hänsch, B. Couillaud, *Optics Comm.* 35 (1980) 441.
- [18] A. Ashkin, G.D. Boyd, J.M. Dziedzic, *IEEE J. Quantum Electron.* QE-2 (1966) 109.
- [19] S. Bourzeix, M.D. Plimmer, F. Nez, L. Julien, F. Biraben, *Optics Comm.* 99 (1993) 89.